Towards continuous monitoring of TNF-α at picomolar concentrations using biosensing by particle motion

Biosensors and Bioelectronics 249 (2024) 115934

Contents lists available at ScienceDirect

Biosensors and Bioelectronics

journal homepage: www.elsevier.com/locate/bios

Towards continuous monitoring of TNF-α at picomolar concentrations using biosensing by particle motion

Alissa D. Buskermolen [a,b], Claire M.S. Michielsen [a,b], Arthur M. de Jong [b,c], Menno W. J. Prins [a,b,c,d,*]

[a] Department of Biomedical Engineering, Eindhoven University of Technology, Eindhoven, the Netherlands
[b] Institute for Complex Molecular Systems (ICMS), Eindhoven University of Technology, Eindhoven, the Netherlands
[c] Department of Applied Physics, Eindhoven University of Technology, Eindhoven, the Netherlands
[d] Helia Biomonitoring, Eindhoven, the Netherlands

ARTICLE INFO

Keywords:
Biosensors
Immunomonitoring
High-affinity binders
Sandwich immunosensor
Particle-based sensing

ABSTRACT

The ability to continuously monitor cytokines is desirable for fundamental research studies and healthcare applications. Cytokine release is characterized by picomolar circulating concentrations, short half-lives, and rapid peak times. Here, we describe the characteristics and feasibility of a particle-based biosensing technique for continuous monitoring of TNF-α at picomolar concentrations. The technique is based on the optical tracking of particle motion and uses an antibody sandwich configuration. Experimental results show how the analyte concentration influences the particle diffusivity and characteristic response time of the sensor, and how the sensitivity range depends on the antibody functionalization density. Furthermore, the data clarifies how antibodies supplemented in solution can shorten the characteristic response time. Finally, we demonstrate association rate-based sensing as a first step towards continuous monitoring of picomolar TNF-α concentrations, over a period of 2 h with delay times under 15 min. The insights from this research will enable the development of continuous monitoring sensors using high-affinity binders, providing the sensitivity and speed needed in applications like cytokine monitoring.

1. Introduction

The biological significance of cytokines and their usefulness for clinical decision making have been studied extensively (Fig. 1A) (B. M. Liu et al., 2021; C. Liu et al., 2021). Cytokines are a broad category of small proteins (~5–20 kDa) that play a key role in cell signaling and are secreted by a wide variety of cell types in response to trauma, infection and inflammation (Dembic, 2015; Kany et al., 2019). Cytokines are generally measured using laboratory-based sandwich immunoassays, in well plate and particle-based assay formats (C. Liu et al., 2021). The measurements involve sample collection, transportation to a laboratory, sample preparation, and then multiple assay steps. The total turnaround time is hours at minimum but can easily take a day or more (Fig. 1B).

Studies have shown that cytokine release can be rapid: cellular immune responses are activated typically within minutes to hours after being triggered (Marshall et al., 2018; Netea et al., 2019). Circulating tumor necrosis factor α (TNF-α) levels, for example, can shift from femtomolar to high picomolar concentrations within 2 h following an inflammatory stimulus (Kiers et al., 2019; Kox et al., 2014). However, limited research data is available about rapid cytokine dynamics due to limitations in measurement technology. Furthermore, the long turnaround times in present clinical analysis preclude the development of intervention protocols based on rapid changes of cytokine levels. This calls for the development of analysis technologies that can continuously record cytokine concentration-time profiles, for achieving a better understanding of cytokine dynamics, e.g. through pre-clinical organoid studies (Dekkers et al., 2023), and for enabling prompt treatment of patients with fluctuating inflammatory conditions (Fig. 1C) (Cao et al., 2018; Chen et al., 2015; Clifford et al., 2021).

Recently, we described a continuous biosensing technique based on tracking the motion of freely diffusing particles near a sensor substrate, which is referred to as f-BPM, biosensing by free particle motion (Fig. 1D) (Buskermolen et al., 2022). Particles and substrate are functionalized with binder molecules, and analyte molecules change the motion properties of the particles. The f-BPM sensor technology was demonstrated for the continuous monitoring of ssDNA and cortisol,

* Corresponding author. Department of Biomedical Engineering, Eindhoven University of Technology, Eindhoven, the Netherlands.
E-mail address: m.w.j.prins@tue.nl (M.W.J. Prins).

https://doi.org/10.1016/j.bios.2023.115934
Received 23 August 2023; Received in revised form 30 November 2023; Accepted 13 December 2023
Available online 14 December 2023

using binder molecules with relatively high dissociation rates and low affinities (Buskermolen et al., 2022). However, cytokines are present at low concentrations and available antibodies have high affinities and low dissociation rates (Landry et al., 2015; Yang et al., 2016), which changes the kinetic properties and requires novel concepts to be able to realize sensors for continuous monitoring.

Here, we study how the continuous monitoring of TNF-α at picomolar concentrations can be achieved by measuring association rates. We study the kinetic properties of f-BPM TNF-α measurements using commercially available antibodies. The dependencies of the sensitivity range on the antibody density in the sensor are studied. The data clarifies how the sensor kinetics depend on analyte and antibody concentrations and how antibodies supplemented in solution can be used to shorten the characteristic response time. A first step towards the monitoring of TNF-α is demonstrated, with a delay time of less than 15 min over an accumulated measurement time of 2 h. Finally, we summarize how sandwich-format continuous monitoring biosensors can be realized using high-affinity binders with slow dissociation rates.

2. Materials and methods

2.1. Materials

Polystyrene sheets (300 mm × 300 mm, thickness 1.2 mm) were obtained from Goodfellow Corporation (ST31-SH-000120) and cut to 25 mm × 75 mm. Custom-made fluid cell stickers with internal volume ~20 μl and chamber height 450 μm were obtained from Grace Biolabs (USA). TNF-α monoclonal antibodies mAb1, mAb11, and biotinylated mAb11 (eBioscience), Phosphate Buffered Saline (PBS) tablets, Tween-20, bovine serum albumin (BSA), sodium carbonate and sodium bicarbonate (anhydrous) were purchased from Sigma-Aldrich. The mAb1 and mAb11 antibodies form a sandwich pair developed for ELISA. Human recombinant TNF-α was obtained from Sino Biological. Nunc MaxiSorp clear flat-bottom 96-well plates (Invitrogen) and Dynabeads MyOne Streptavidin C1 (Invitrogen) were purchased from ThermoFisher Scientific. mPEG-biotin (MW 1 kDa) was purchased from Nanocs (USA).

2.2. 96-well plate screening

50 μl of 10 nM mAb1 in 0.1M sodium carbonate-bicarbonate buffer (CB; pH 10) were added to a 96-well plate and incubated for 2h. All incubations for all experiments were performed at room temperature.

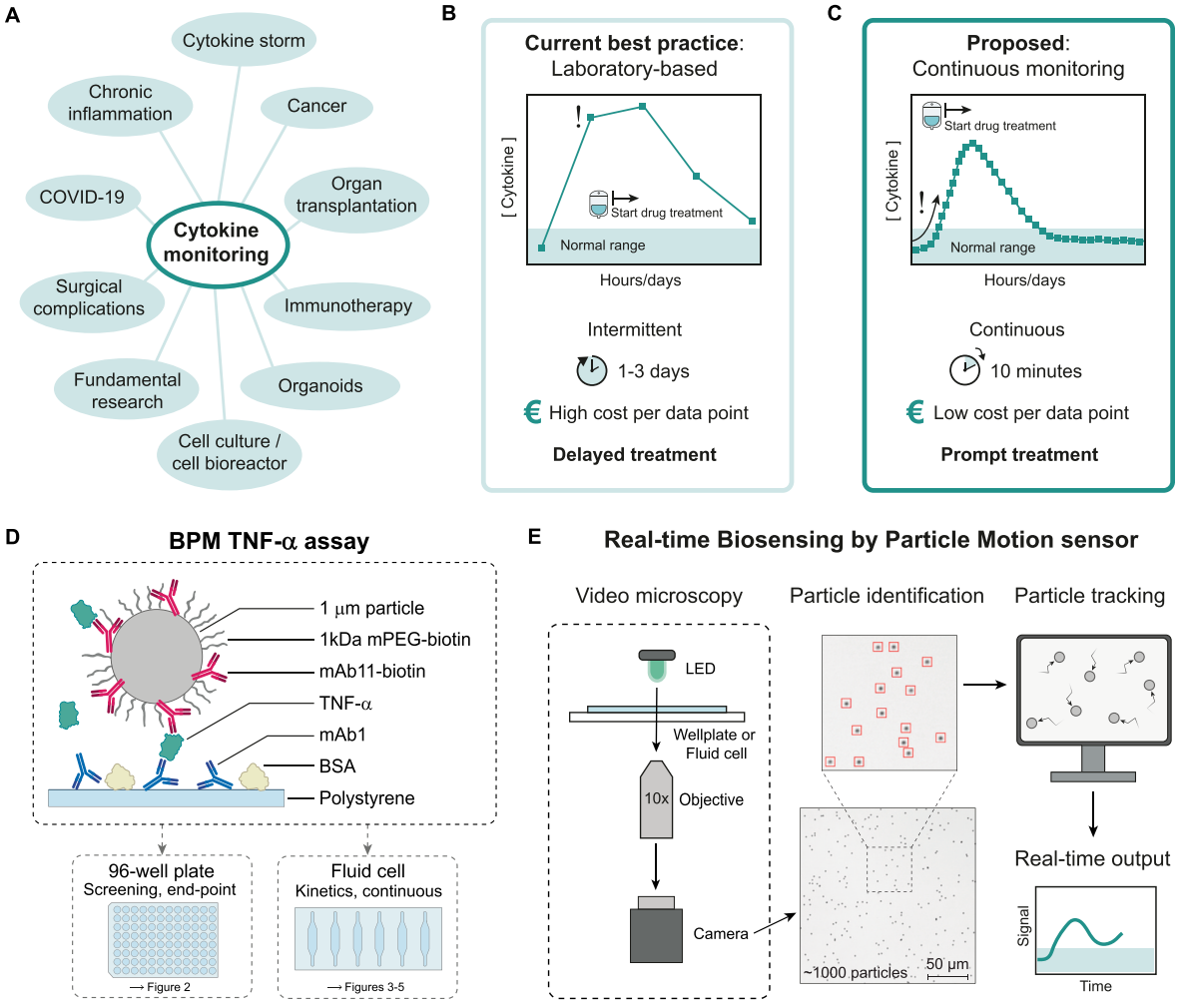

Fig. 1. Cytokine monitoring using biosensing by particle motion. (A) Applications of cytokine monitoring. (B) The current best practice of measuring cytokine levels in the clinic. (C) The proposed method of measuring cytokine levels: continuous monitoring. (D) Biosensing by free particle motion (f-BPM): a particle-based continuous biosensing approach for the cytokine TNF-α using an antibody sandwich format. The particle motion is influenced by the TNF-α concentration in solution. 96-well plates were used to screen reagent conditions, and fluid cells for kinetic and continuous measurements. (E) Particles were visualized using a home-built microscopy setup with a high-speed camera. Dedicated software was used to track the positions of ~1000 particles simultaneously in real-time.

Wells were emptied and 50 μl 1% BSA in PBS was added and incubated for 1h. 2 μl of 10, 25, 50 or 100 nM biotin-mAb11 in PBS were mixed with 2 μl of particles (1 μm; 10 mg/mL), incubated for 45 min on a rotating fin, and blocked with, 40 μl 100 μM mPEG-biotin in PBS for 15 min. The particles were washed 3x with 200 μl PBS using magnetic separation. Next, 200 μl 1% BSA in PBS was added and incubated for 1h. The solutions were sonicated (10x, 70% amplitude, 0.5s duty cycle; Hielscher UIS250V, Ultrasound Technology), and diluted 15 times in buffer (0.1% BSA, 0.005% Tween-20 in PBS). Wells were emptied and 25 μl of particle solutions were added to specific wells. TNF-α was diluted in buffer to 6.25–3200 pM (two-fold serial dilution), 25 μl was added to specific wells (in triplicate) and incubated for 3h. Particle motion was recorded for 30 s in each well. The plate was measured three times.

2.3. Kinetic measurements in separate fluid cells

Six fluid cell stickers (for details see Fig. S2) were attached to a polystyrene slide. 50 μl 10 nM mAb1 in CB was added to each fluid cell and incubated for 2h. 50 μl 1% BSA in PBS was added to each fluid cell and incubated for 1h. Particles were functionalized with 50 nM biotin-mAb11 as described before. 50 μl of particle solutions were added to each fluid cell, inlets and outlets were sealed with tape, and particles were left to sediment for ~10 min. TNF-α was diluted to 6.25–200 pM (two-fold dilution), and 50 μl were added to each separate fluid cell using a multi-pipette. Measurements were started immediately. Particle motion was recorded in 30-s periods. Time-dependent data was recorded in parallel in six fluid cells on a single slide, by scanning the slide with respect to the optical imaging system.

2.4. Kinetic measurements with supplemented binders in separate fluid cells

Samples were prepared as described in section "Kinetic measurements in separate fluid cells", using 10 nM biotin-mAb11 for particle functionalization. TNF-α was diluted to 100–600 pM. TNF-α monoclonal antibody mAb11 was diluted to 2.5–40 nM (two-fold dilution). Immediately before addition to the fluid cells, TNF-α and mAb11 samples were mixed 1:1. Reference TNF-α samples were not mixed with mAb11. 50 μl samples were added to the fluid cells using a multi-pipette and measurements were started immediately. Particle motion was recorded in 30-s periods.

2.5. Serial measurements in a single fluid cell

Samples were prepared as described in section "Kinetic measurements in separate fluid cells". 40 μl samples (0–400 pM TNF-α) were added sequentially to the fluid cell, and for each concentration the particle motion was recorded for 10 min in 30-s blocks (increasing concentrations) or 5 min in 15-s blocks (alternating concentrations).

2.6. Data acquisition and processing

Measurements were performed with a custom-built microscope with motorized XY stage (ASR series, 100 mm × 120 mm travel; Zaber Technologies Inc.) using brightfield illumination (12V, 3 mm green LED) and 10x magnification (10x DIN Achromatic Finite Intl Standard Objective (Edmund Optics)). Particle motion was recorded in 15- to 30-s blocks at 60Hz using a high-speed camera (Sony Blackfly S BFS-U3-31S4M) with a field of view of 2048x1536 pixels (706 μm × 530 μm). Autofocusing was performed between each measurement block using a miniature linear actuator (Zaber T-LA13A). The microscope was controlled using MATLAB. Particle positions were tracked in real-time using dedicated particle tracking software (Bergkamp et al., 2023) which applies two-dimensional phasor-based localization (Martens et al., 2018). Unbound and bound states were distinguished based on a diffusivity threshold at 0.12 $\mu m^2/s$. The bound fraction is defined as the ratio between the population of bound states and the total population of states over time (see also Fig. S1).

Bound fraction dose-response curves were fitted using a sigmoidal logistic function to extract EC50 values:

$$BF = y_{max} + (y_{min} - y_{max}) / (1 + (C_a/EC50)^p) \quad \text{(Eq. 1)}$$

where y_{min} is the bottom plateau, y_{max} the top plateau, C_a the TNF-α concentration, and p the slope factor.

Kinetic association curves were fitted with an exponential plus linear model (see Main Text and Fig. S6 for details):

$$S(t) = S_0 + \Delta S^*(1 - \exp(-(t - t_0)/\tau)) + b^*t \quad \text{(Eq. 2)}$$

with S_0 the signal at $t = 0$ of the measurement, and ΔS the amplitude of the exponential response. The final signal (plateau) of the exponential part of the association curve is defined as $S_{end} = S_0 + \Delta S$. τ is the characteristic response time and t_0 is the starting point of the exponential curve. b represents the slope of the secondary linear part of the signal.

Characteristic response time curves as a function of analyte concentration C_a were fitted with a reciprocal function to obtain the apparent association rate $k_{on,app}$ and apparent dissociation rate $k_{off,app}$:

$$\tau = 1 / (k_{on,app}{}^*C_a + k_{off,app}) \quad \text{(Eq. 3)}$$

Characteristic response time curves as a function of the supplemented binder concentration $C_{b,suppl}$ were fitted with a reciprocal function adapted from Eq. (3) to obtain the apparent antibody association rate $k_{on,app}$:

$$\tau = 1 / (k_{on,app}{}^*(C_{b,0} + C_{b,suppl})) \quad \text{(Eq. 4)}$$

where $C_{b,0}$ relates to the effective volumetric analyte binding capacity present in the sensor in absence of supplemented binders.

Sequential measurements were fitted with a linear equation to extract the observed rate k_{obs} (slope). However, due to the low k_{off} of the sandwich mAb1/TNF-α/mAb11 complex, a particle once bound remains bound during the remainder of the experiment, so does not contribute anymore to an analyte-dependent signal. Therefore, a corrected rate parameter was defined, $k_{obs,corr}$, which takes account of the fraction of particles that is still able to respond to analyte ($1 - BF_{start}$):

$$k_{obs,corr} = k_{obs} / (1 - BF_{start}) \quad \text{(Eq. 5)}$$

where BF_{start} is the bound fraction at the start of each measurement series.

3. Results and discussion

3.1. Sensing principle and tuning of the sensor conditions

The f-BPM sensing concept relies on the continuous tracking of the Brownian motion of biofunctionalized particles hovering over a biofunctionalized sensor substrate (Buskermolen et al., 2022). In Fig. 1D, the molecular details of the f-BPM TNF-α sandwich immunosensor are sketched (more details provided in Table S1). Streptavidin-coated particles with a diameter of 1 μm were functionalized with biotinylated anti-TNF-α mAb11 antibodies ('particle-side binders', coupled at concentration $[B]_{Particle}$) and blocked with biotin-mPEG to reduce non-specific interactions with the substrate. A polystyrene substrate was coated with anti-TNF-α mAb1 antibodies ('substrate-side binders') via physisorption and blocked with BSA. The sensor was studied in 96-well plates to screen reagent conditions (Fig. 2) and in fluid cells for kinetic and continuous measurements (Figs. 3–5). Particle motion was recorded using a custom-built microscopy setup with a high-speed camera (Fig. 1E). Particle positions were tracked in real time using dedicated

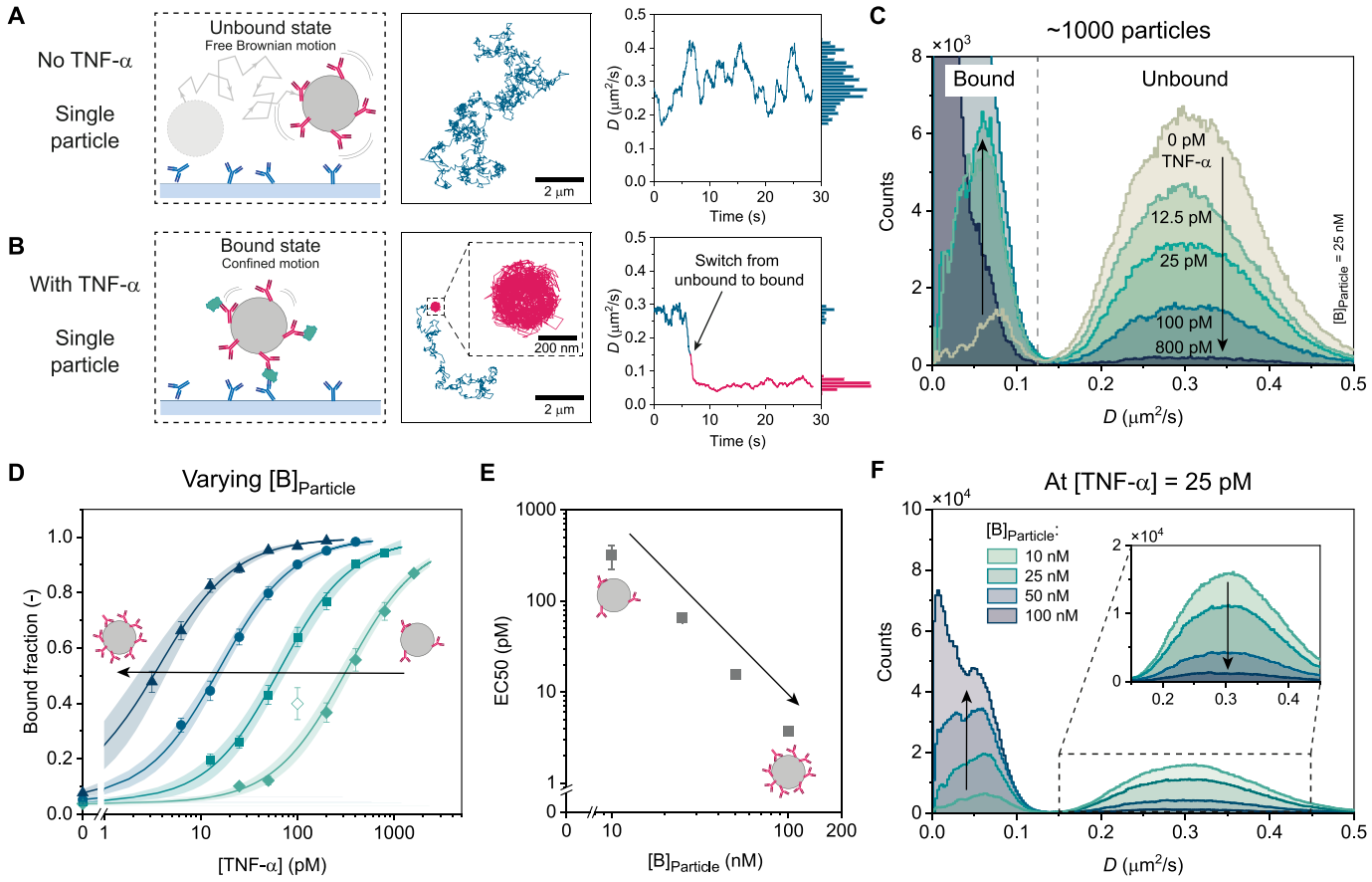

Fig. 2. Study of sensor conditions using 96-well plate experiments. (A) At low TNF-α concentrations, the particles dominantly exhibit free Brownian motion (unbound state). The diffusivity (D) time trace shows a broad distribution in D around 0.3 $\mu m^2/s$. (B) At higher TNF-α concentrations particles become confined in their motion due to the sandwich complex formation, resulting in a circular motion pattern. In the diffusivity time trace the D decreases to ~0.05 $\mu m^2/s$ with a narrow distribution. (C) Ensemble diffusivity distributions of ~1000 particles. A threshold at $D = 0.12$ $\mu m^2/s$ (dashed line) was used to distinguish unbound from bound states. With increasing TNF-α concentrations the unbound population decreases while the bound population increases and shifts to lower diffusivity values due to multivalent binding. The ratio between the population bound and the total population is the bound fraction. (D) Tuning sensor response range by varying the particle-side binder concentration $[B]_{Particle}$. Particle-side binder concentrations (left to right): 100, 50, 25 and 10 nM. Data were fitted using Eq. (1) to obtain the EC50 values (fits constrained between 0 and 1). Data represent mean ± SE (triplicate wells, three timepoints). (E) EC50 values obtained from the fits in panel D. A two-fold increase of $[B]_{Particle}$ corresponds with a ~4x decrease in EC50. Error bars depict fitting errors based on a 68% confidence interval. (F) At [TNF-α] = 25 pM the diffusivity distributions show a clear dependency on the particle-side binder density.

particle tracking software (Bergkamp et al., 2023). A motorized sample stage enabled automated measurements by scanning 96-well plates or multiple individual fluid cells and ensured the observed field-of-view (FOV) was consistent over time.

In the absence of TNF-α the particles mainly experience free Brownian motion (Fig. 2A). Particle x,y-trajectories were translated into diffusivity (D) time traces (Fig. 2A, right), showing D around 0.3 $\mu m^2/s$ in the unbound state. TNF-α (monomeric) can bind to the particle- and substrate-side binders, and a sandwich complex can be formed between the particle and the substrate, resulting in a decrease in diffusivity to ~0.05 $\mu m^2/s$ (bound state; Fig. 2B). Fig. 2C shows diffusivity distributions of ~1000 particles. For increasing TNF-α concentrations the characteristic unbound peak decreases, while the bound peak increases and shifts to lower diffusivity values due to an increasing contribution of multivalent binding. Unbound and bound states can be distinguished using a threshold at $D = 0.12$ $\mu m^2/s$ (dashed line). The main readout parameter of the TNF-α f-BPM immunosensor is the bound fraction, which is defined as the ratio between the number of measured diffusivity values (counts) below the diffusivity threshold (related to bound states) and the total number of measured diffusivity values (Fig. S1). These numbers are summations for all particles that are tracked in the FOV, for a given measurement frequency and total observation time.

Fig. 2D shows how the sensor response range can be tuned by changing the particle-side binder density (see also Fig. S3). With increasing binder densities (higher $[B]_{Particle}$), the dose-response curves shift to lower TNF-α concentrations. The curves were fitted using Eq. (1) and characterized by their EC50 values. Fig. 2E shows how the EC50 depends on $[B]_{Particle}$. The scaling is also clear in the diffusivity distributions at [TNF-α] = 25 pM, as can be seen in Fig. 2F. With increasing $[B]_{Particle}$ the unbound population decreases while the bound population increases. Besides the high sensitivity, the f-BPM TNF-α sensor also showed excellent specificity and selectivity in the presence of several different cytokines (Fig. S4). In these 96-well plate experiments incubation times of 3 h were used to limit the influence of time on the sensor response. In the next Section, experiments on analyte-dependent response kinetics are presented, for a constant density of particle-side binders ($[B]_{Particle} = 50$ nM).

3.2. Time-dependent curves: analyte-dependent kinetics

Fig. 3 shows the analyte-dependent kinetics of an f-BPM TNF-α sandwich immunosensor with 10 nM substrate-side binder and 50 nM particle-side binder (see also Fig. S5). The association curves in Fig. 3A show the change in bound fraction over time for TNF-α concentrations

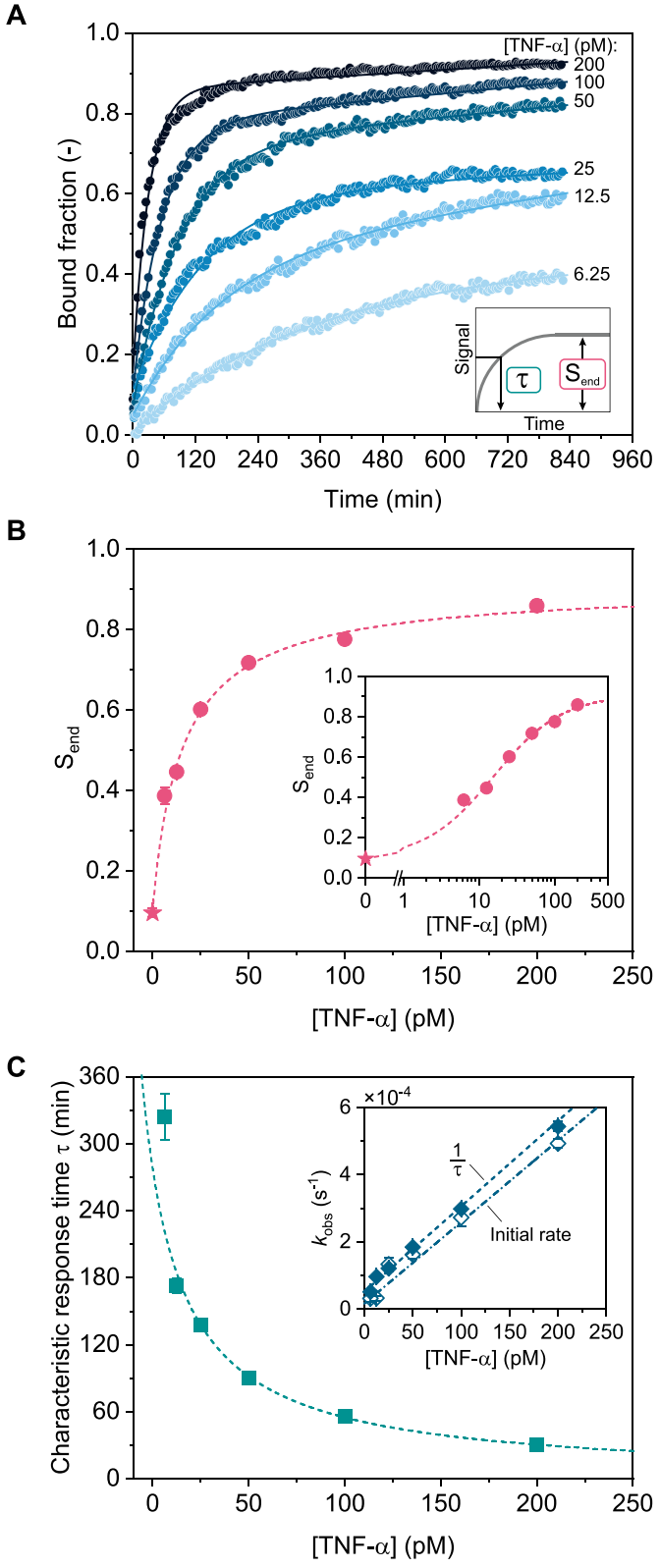

(caption on next column)

Fig. 3. Analyte-dependent kinetics of the f-BPM TNF-α sensor. (A) Bound fraction as a function of time for TNF-α concentrations from 6.25 to 200 pM. Data were fitted using Eq. (2) to extract the characteristic response time τ and the final signal S_{end}. Inset: τ represents the characteristic time to approach the end condition; the final signal S_{end} corresponds to the plateau of the exponential part of the association curve. 10 nM substrate-side binder and 50 nM particle-side binder were used. (B) Dose-response curve with S_{end} as a function of TNF-α concentration. Blank datapoint (star) is the average of the blank signals of six separate fluid cells. Inset: dose-response curve with a logarithmic concentration axis. Data was fitted using Eq. (1) (dashed line) giving EC50 = 16 ± 3 pM (fit constrained between 0 and 1). (C) Characteristic response time τ as a function of TNF-α concentration. Data was fitted with Eq. (3) (dashed line), giving $k_{on,app} = 2.4 \pm 0.1{\cdot}10^{6}$ $M^{-1}s^{-1}$ and $k_{off,app} = 6.0 \pm 0.7{\cdot}10^{-5}$ s^{-1}. Inset: observed rate k_{obs} as a function of TNF-α concentration. Filled diamonds: $k_{obs} = 1/\tau$; open diamonds: k_{obs} obtained by linear fitting of the first 5 datapoints in panel A. Fitting with the reciprocal of Eq. (3) gives $k_{on,app} = 2.5 \pm 0.2{\cdot}10^{6}$ $M^{-1}s^{-1}$ and $k_{off,app} = 5.2 \pm 0.8{\cdot}10^{-5}$ s^{-1} (dashed line), and $k_{on,app} = 2.4 \pm 0.1{\cdot}10^{6}$ $M^{-1}s^{-1}$ and $k_{off,app} = 1.7 \pm 1.1{\cdot}10^{-5}$ s^{-1} (dash-dotted line). Errors are fitting errors based on a 68% confidence interval.

ranging from 6.25 to 200 pM. By fitting the data with Eq. (2), the characteristic response time τ and final signal S_{end} could be extracted (inset Fig. 3A). The time-dependent curves closely follow the behavior of Eq. (2): a sum of a single exponential and a linear function. The single-exponential time-dependent function $(1 - e^{-t/\tau})$ corresponds to the mathematical solution of a first-order two-component reaction, with τ the characteristic time to approach the end condition. The final signal S_{end} corresponds to the plateau value of the exponential function, with $S_{end} = S_0 + \Delta S$. The linear function in Eq. (2) represents slow binding processes between particles and substrate that do not saturate on the timescale of the measurements (Fig. S6).

To understand the time-dependent response, let us consider the pathways how particle-analyte-substrate sandwich complexes are formed in the immunosensor: (1) an analyte molecule binds first to a particle, and then the particle-analyte complex binds to the substrate, indicated as pathway A-AP-SAP, or (2) an analyte molecule binds first to the substrate, and subsequently a particle binds to the substrate-analyte complex, indicated as pathway A-AS-SAP (Fig. S7). Both pathways consist of two sequential binding reactions, involving first analyte diffusion and capture, and subsequently particle diffusion and complex formation (Fig. S7). The characteristic response time of the biosensor is determined by the slowest sub-reaction in the dominant pathway.

We studied sub-reactions AP-SAP and AS-SAP by pre-incubating particles or substrate with analyte (Fig. S8). The data show that reaction AP-SAP results in a ~4 times smaller τ than reaction AS-SAP, indicating that a sandwich complex is formed faster when an analyte molecule binds first to a particle instead of to the substrate. Furthermore, the data show that the τ values of these pre-incubated reactions are at least four times smaller than the characteristic response time of the sandwich immunosensor in Fig. 3. This implies that sub-reactions AP-SAP and AS-SAP are not limiting the biosensor response, and that it is sub-reaction A-AS and/or A-AP that limits the biosensor response. These sub-reactions represent reaction-diffusion processes, where analyte diffusion as well as analyte reaction play a role. The importance of reaction versus diffusion can be estimated from the Damköhler number (D_a, see Table S1), which describes the ratio between the reaction rate and the diffusion rate (Lubken et al., 2021). A low value ($D_a \ll 1$) means that the kinetics are reaction-limited, whereas a high value ($D_a \gg 1$) means that the kinetics are diffusion-limited. For the f-BPM sensor in Fig. 3, we estimate that D_a could be of the order of one, indicating that both diffusion and reaction may play a role in the observed overall rate of the reaction (Lubken et al., 2021). We cannot yet say which of the two pathways (A-AP-SAP or A-AS-SAP) dominates the exponential response or which contributes to the secondary linear response. Pathway A-AS-SAP might be dominant, due to the higher total number of binders on the substrate (Table S1). Conversely, pathway A-AP-SAP might lead

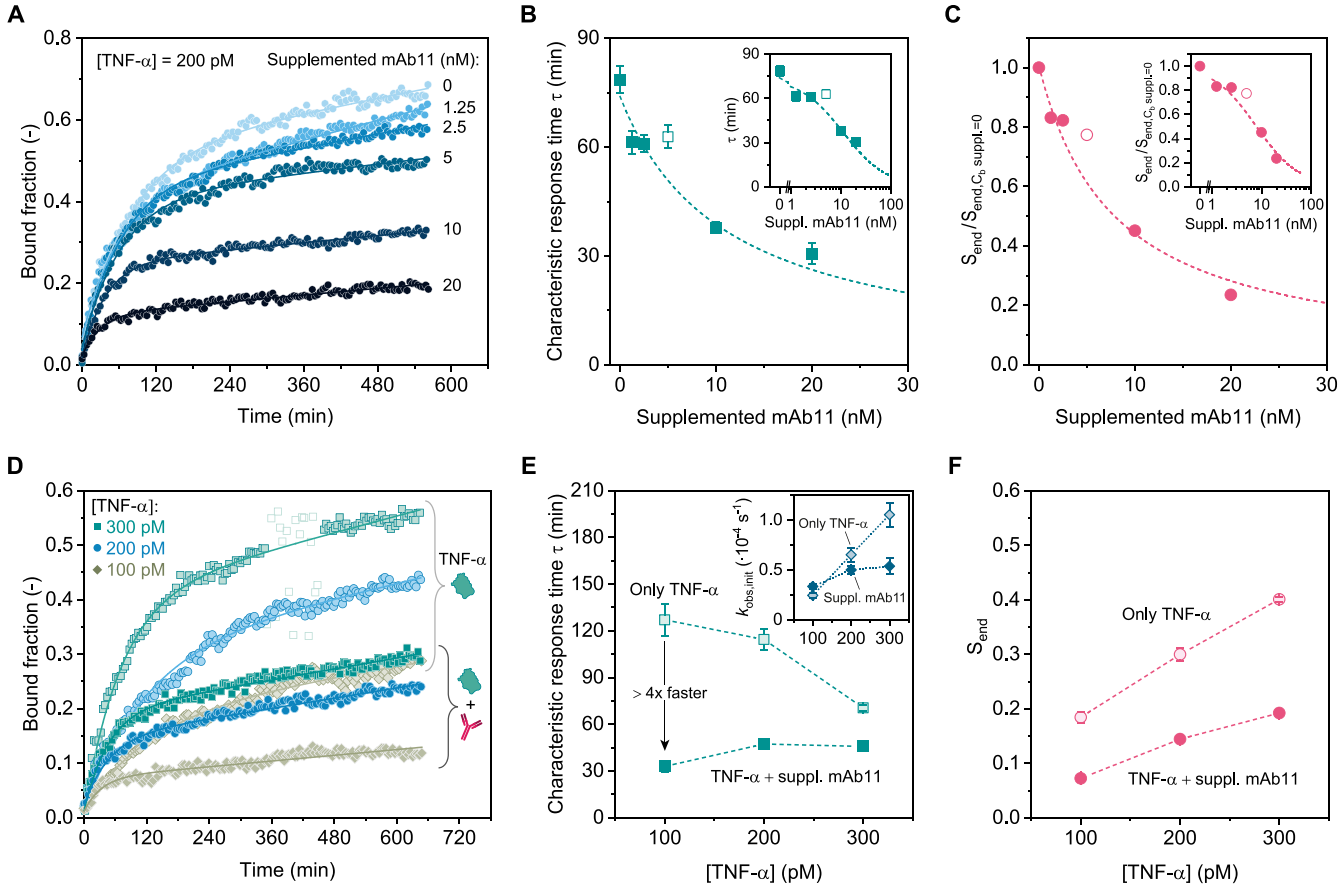

Fig. 4. Accelerating sensor kinetics by supplementing binders in solution. (A) Association curves at [TNF-α] = 200 pM, with 0–20 nM of mAb11 supplemented in solution. Data were fitted with Eq. (2) to extract τ and S_{end}. (B) The τ decreases with increasing concentrations of mAb11 supplemented in solution. Inset: the same data on a semi-log scale. Data were fitted with Eq. (4) (dashed line), giving $k_{on,app} = 2.1 \pm 0.3{\cdot}10^4$ $M^{-1}s^{-1}$ and $C_{b,0} = 11 \pm 2$ nM. (C) Dose-response curve depicting the difference in signal with respect to the initial S_{end} at 200 pM TNF-α without supplemented mAb11 ($S_{end,C_b\ suppl.=0}$). Inset: the same data on a semi-log scale. Dashed lines are a guide to the eye. (D) Association curves at 100, 200 and 300 pM TNF-α without (open markers) and with 10 nM supplemented mAb11 (solid markers). Data were fitted with Eq. (2) to extract τ and S_{end}. (E) τ as a function of TNF-α concentration, without (open markers) and with (solid markers) supplemented mAb11. With supplemented mAb11, τ becomes smaller and independent of TNF-α concentration. Inset: initial rate ($k_{obs,init}$) obtained by linear fitting of the initial phase of each association curve. (F) S_{end} as a function of TNF-α concentration, without (open markers) and with (solid markers) supplemented mAb11. In both cases S_{end} depends on the TNF-α concentration. Errors are fitting errors based on a 68% confidence interval. 10 nM substrate-side binder and 10 nM particle-side binder were used.

to a faster observable response, given that AP-SAP is faster than AS-SAP. This is a topic that we will study in follow-up research.

Fig. 3B shows the dose-response curve expressed as the final signal S_{end}. Fitting the data using Eq. (1) (dashed line) gives an EC50 of 16 ± 3 pM. The τ also depends on the TNF-α concentration: higher analyte concentrations result in a smaller τ (Fig. 3C). The data is fitted (dashed line) using Eq. (3), which gives an apparent association rate $k_{on,app}$ of $2.4 \pm 0.1{\cdot}10^6$ $M^{-1}s^{-1}$ and an apparent dissociation rate $k_{off,app}$ of $6.0 \pm 0.7{\cdot}10^{-5}$ s^{-1}. $k_{on,app}$ describes the analyte-concentration dependence of the average rate at which individual particles bind to the surface, and $k_{off,app}$ describes the spontaneous dissociation of particles from the surface. The inset in Fig. 3C shows the observed rate k_{obs} as a function of analyte concentration, where filled diamonds depict $k_{obs} = 1/\tau$.

The initial slopes of the kinetic curves in Fig. 3A can also be used to extract observed rates (Fig. S9). The open diamonds in Fig. 3C depict k_{obs} obtained by linear fitting of the first five datapoints of the association. The data closely follow the k_{obs} obtained by fitting the full association curve (filled diamonds), and fitting with the reciprocal of Eq. (3) (dash-dotted line) gives a $k_{on,app}$ of $2.4 \pm 0.1{\cdot}10^6$ $M^{-1}s^{-1}$ and $k_{off,app}$ of $1.7 \pm 1.1{\cdot}10^{-5}$ s^{-1}. These values closely resemble those found above, indicating that fitting of the initial phase gives a good approximation of the observed rate (Table S2).

When fitting the full association curves, a $k_{off,app}$ of $\sim 5{\cdot}10^{-5}$ s^{-1} was observed, indicating that particle dissociation is slow ($1/k_{off,app} \cong 6$ hours). This can be attributed to both molecular and particle properties. The antibodies have high affinities and low dissociation rate constants, typically in the range 10^{-6}–10^{-4} s^{-1} (Landry et al., 2015; Yang et al., 2016). In addition, the low diffusivity of analyte-particle complexes can increase the rebinding probability, and at high analyte concentrations particles may exhibit multivalent interactions. The measurement data show characteristic response times of an hour or more at low TNF-α concentrations, which could strongly limit clinical applications given the rapid peak times of TNF-α (Kiers et al., 2019; Kox et al., 2014; Yiu et al., 2012). Thus, the sensor needs to be accelerated, which is addressed in the next Sections.

3.3. Time-dependent curves: binder-dominated kinetics

A recently proposed approach to accelerate an immunosensor based on high-affinity binder molecules, is by designing a limited-volume sensor with binder-dominated kinetics (Fig. S10) (Lubken et al., 2021). Assume a bi-molecular affinity reaction between analyte A and binder B taking place in a limited reaction volume, without refreshing

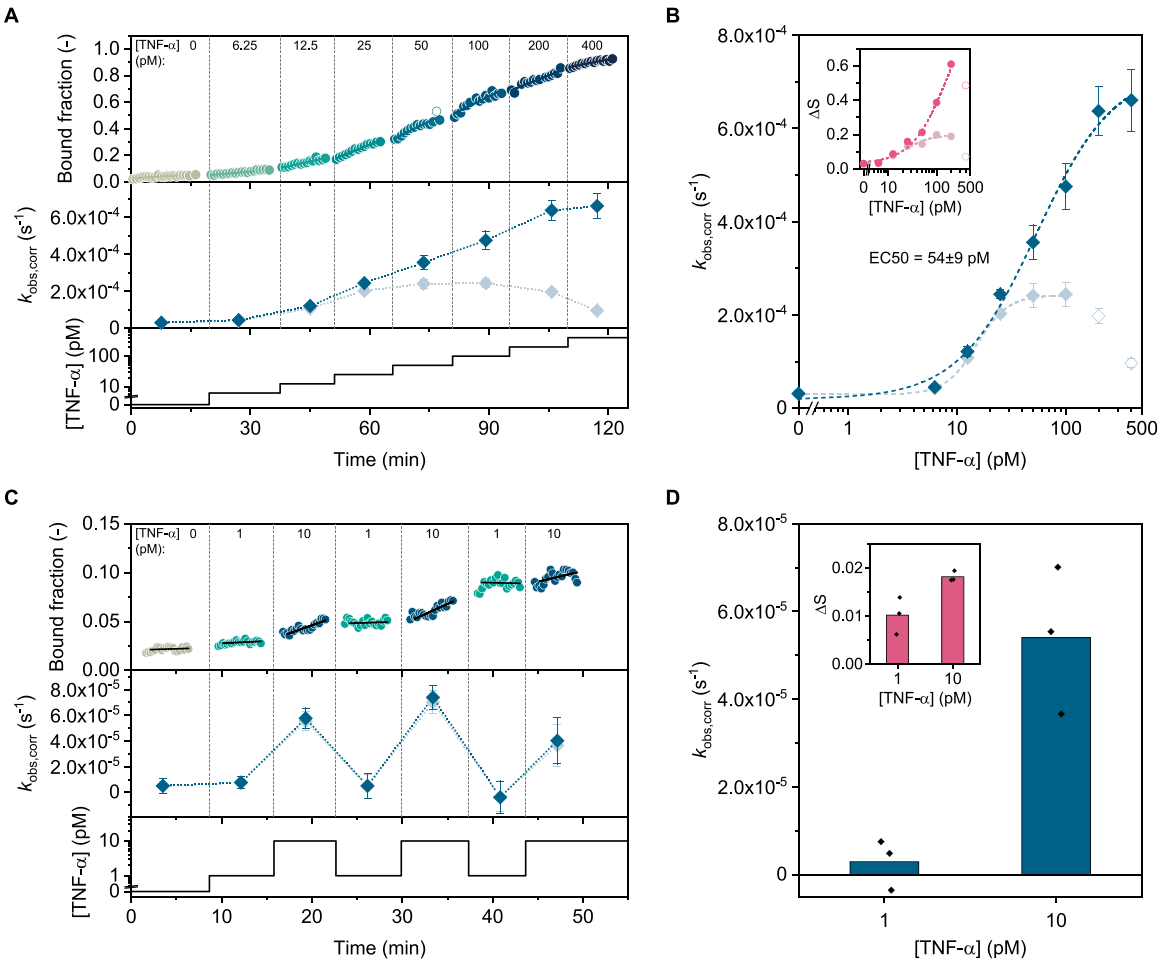

Fig. 5. Demonstration of dynamic monitoring of TNF-α with high time resolution using f-BPM. (A) Response in bound fraction (top panel) to stepwise increasing concentrations of TNF-α (bottom panel). Linear fitting of the first fifteen datapoints of each measurement series yielded the observed rate k_{obs} (light grey diamonds, middle panel). k_{obs} was corrected using Eq. (5). The $k_{obs,corr}$ are depicted as dark blue diamonds. (B) Dose-response expressed as the observed rate, with original (light grey diamonds) and corrected data (dark blue diamonds). Dashed lines indicate sigmoidal fits (Eq. (1)). For the corrected data the EC50 = 54 ± 9 pM. Inset: response expressed as Δ*S*. Dashed lines serve as guide to the eye. (C) Response in bound fraction (top panel) to TNF-α concentrations alternating between 1 and 10 pM (bottom panel). Linear fitting yields a k_{obs} for each 5-min measurement (light grey diamonds, middle panel). The first two datapoints of each measurement series were omitted in the fits. k_{obs} was corrected using Eq. (5) (dark blue diamonds). (D) Response in $k_{obs,corr}$ and Δ*S* (inset) for 1 and 10 pM TNF-α. Bars represent the mean of the three measurements depicted in panel C (individual datapoints overlayed). The errors are fitting errors based on a 68% confidence interval. 10 nM substrate-side binder and 50 nM particle-side binder were used.

the fluid. While the binding reaction between A and B occurs, the concentration of free analyte molecules in solution changes as a function of time ($C_a^{t=\infty} \neq C_a^{t=0}$), which affects the equilibrium state as well as the characteristic response time of the sensor.

A bi-molecular limited-volume affinity reaction in reaction-limited conditions (where transport effects can be ignored) has a characteristic response time τ that is determined by the highest of the three parameters K_d, C_a, and C_b, i.e. the equilibrium dissociation constant K_d and the starting values of the analyte and binder concentrations C_a and C_b respectively (Roberts, 2013). If K_d is highest, then $\tau \cong 1/k_{off}$; if C_a is highest, then $\tau \cong 1/(C_a k_{on})$; and if C_b is highest, then $\tau \cong 1/(C_b \cdot k_{on})$. The latter condition is referred to as binder-dominated kinetics, where τ decreases with an increasing value of the binder concentration, as a result of analyte depletion (Fig. S10) (Lubken et al., 2021). In a BPM sensor, the effective concentration of binder molecules can be increased by coupling more antibodies to substrate and particles, or by supplementing binder molecules in solution (Fig. S10), as was previously demonstrated experimentally for a tethered-BPM oligonucleotide sensor (Lubken et al., 2021). Here, we study how antibodies (mAb11) supplemented in solution influence τ and S_{end} in the TNF-α immunosensor (Fig. 4).

Various concentrations of mAb11 (1.25–20 nM) were added in solution to a sample with 200 pM TNF-α, and the response was measured over time (Fig. 4A, Fig. S11). The data show that the signal decreases with increasing supplemented mAb11 concentration. Fitting the data using Eq. (2) gives the τ and S_{end} values. Fig. 4B shows that τ decreases as expected with increasing supplemented mAb11 concentration, with $\tau \cong 1/(C_b \cdot k_{on})$. This indicates that it is possible to decrease the characteristic response time of a sandwich-type immunosensor, by supplying excess binder molecules in solution. The data was fitted with Eq. (4) (dashed line) giving a $k_{on,app}$ of $2.1 \pm 0.3 \cdot 10^4$ $M^{-1}s^{-1}$. Due to the excess of antibodies in solution, this value is related to the association rate per antibody in solution. The effective volumetric binder concentration $C_{b,0}$ obtained from the fit is 11 ± 2 nM. This binding capacity is a sum of specific binding and potential analyte loss due to non-specific binding. Fig. 4C depicts the signal change with respect to the condition without supplemented binders ($C_{b,suppl.} = 0$), showing a decrease in S_{end} with increasing $C_{b,suppl.}$. For the highest $C_{b,suppl.}$ (20 nM) the signal is ~5 times lower compared to the original signal. Thus, there is a tradeoff between speed and sensitivity, which provides opportunities to optimize the sensor for specific applications, for instance by varying the immobilized and supplemented binder concentrations. This tradeoff is discussed in

more detail in Section 4 of the SI.

In a regime with binder-dominated kinetics, τ is expected to become independent of analyte concentration (Lubken et al., 2021). Fig. 4D depicts the results of an experiment in which 10 nM mAb11 was supplied in solution to different concentrations of TNF-α (100, 200 or 300 pM). The curves were fitted with Eq. (2) to obtain the τ and S_{end} values. Fig. 4E shows that τ of samples with only TNF-α (open squares) clearly depend on the analyte concentration. Addition of free mAb11 (solid squares) results in a smaller τ for all TNF-α concentrations, by a factor four in the case of 100 pM TNF-α. Furthermore, the τ values indeed hardly depend on the analyte concentration, in agreement with binder-dominated kinetics. The inset in Fig. 4E shows the observed initial rate $k_{obs,init}$ as a function of TNF-α concentration. $k_{obs,init}$ values were obtained by linear fitting of the initial phase of each association curve. Without supplemented mAb11 the initial rate strongly depends on the analyte concentration. This dependency decreases when mAb11 is supplemented in solution, which is in line with the trends observed earlier in the characteristic response time. Fig. 4F shows the dose-response of S_{end} as a function of TNF-α concentration, with and without supplemented binders, showing that different TNF-α concentrations can clearly be distinguished.

3.4. Dynamic monitoring of TNF-α with high time resolution

The results of the previous Sections show that a measurement of the initial rate can be used to measure picomolar TNF-α levels. In Fig. 5 we demonstrate that this measurement principle can be used to sequentially measure samples with high time resolution. The sensor cartridge geometry and fluidics are discussed in detail in Fig. S2. In Fig. 5A samples with increasing TNF-α concentrations were added to the same fluid-cell sensor. The slopes of linear fits of each 10-min measurement series represent the k_{obs}. The irreversible sensor accumulates TNF-α after each sample addition and therefore the bound fraction gradually increases. The k_{obs} were corrected for the available sensor response range using Eq. (5), because the available range decreases after every sample addition. This yields a corrected observed rate $k_{obs,corr}$, depicted as blue diamonds in Fig. 5A and B (grey datapoints represent the uncorrected rates). In Fig. 5B the dose-response curves of the $k_{obs,corr}$ and the signal change ΔS (inset) are shown (see also Fig. S12). Data were fitted with Eq. (1) to extract the EC50 (dashed line through blue diamonds, EC50 = 54 ± 9 pM), or to serve as a guide to the eye (inset and uncorrected data). The $k_{obs,corr}$ values found here and the k_{obs} values found before (inset of Fig. 3C) all fall in a similar range of ~0.5–7·10^{-4} s^{-1} and show good correspondence for the different TNF-α concentrations. Thus, $k_{obs,corr}$ relates quantitatively to the TNF-α concentration. We believe this is due to the fact that the f-BPM sensor has single-molecule resolution, and operates at low TNF-α concentrations (i.e. most antibodies are not occupied). Overall, the results show that increases in TNF-α concentrations in the low picomolar range can be continuously monitored with a delay time of less than 15 min over an accumulated measurement time of 2 h.

Fig. 5C demonstrates that the immunosensor can be used to resolve increases as well as decreases of TNF-α concentrations in the range of 1–10 pM on timescales of a few minutes. Samples with TNF-α concentrations alternating between 1 and 10 pM were sequentially supplied to a single fluid-cell sensor (see also Fig. S13). The slopes of each 5-min measurement were fitted to obtain the k_{obs} (light grey diamonds, middle panel) and $k_{obs,corr}$ (dark blue diamonds). Fig. 5C shows that the time sequence of measured signals corresponds well with the time sequence of applied TNF-α concentrations. Fig. 5D depicts the observed rate and the signal change ΔS (inset) as a function of TNF-α concentration (datapoints overlayed), showing that the rate varies more strongly with concentration than the signal change. The fact that a decrease in sensor response rate is observed when applying a sample with lower analyte concentration, as opposed to a cumulative buildup, can be attributed to the rate-limiting processes in the sensor. We hypothesize that at low analyte concentrations and short measurement times (5 min), mainly the faster process of particle-analyte complex binding to antibodies on the substrate is observed (pathway AP-SAP; see Fig. S7). By reducing the bulk solution from 10 pM to 1 pM TNF-α, the flux of analyte molecules binding to the particles decreases, and as a result the observed rate also decreases.

The results in this Section represent a first development towards the continuous detection of picomolar TNF-α concentrations using the f-BPM sensing principle, by showing measurements with increases as well as decreases of concentration. The sensor readout is based on measuring the initial rate $k_{obs,initial}$ and the signal change ΔS. With a time-to-result of 5–10 min, the readout method provides a way to use traditional high-affinity antibodies for continuous monitoring purposes.

4. Conclusion

We demonstrated biosensing by free particle motion (f-BPM) combined with high-affinity, slow-dissociating antibodies, and studied the feasibility of continuous monitoring of TNF-α at picomolar levels. The sensor was designed to operate with a gradual accumulation of biomarker molecules in the measurement chamber. A first step towards the monitoring of increasing as well as alternating TNF-α concentrations was demonstrated, measured over a 2-hour period with a delay time of less than 15 minutes. The developed measurement concepts address a fundamental challenge with relevance for studying dynamic systems like cytokine release, which demand high sensitivity and specificity over extended monitoring periods with high time resolution of the measurements.

The sensor design has several tradeoffs that can be investigated further. In particular, the sensor has relationships between speed, sensitivity, and the number of measurements that can be performed on a single sensor. At very low analyte concentrations the characteristic sensor response time is long. One way to accelerate the sensor response is by supplementing binders in solution, but this reduces the signal and therefore the sensitivity. Another way to decrease the time-to-result is by shortening the measurement time and quantifying the initial slope of the response. This allows for rapid, sequential measurements on a single sensor, with biomarker molecules gradually accumulating in the measurement chamber. As molecules accumulate, the measurement range of the sensor decreases, so the sensitivity decreases and the number of samples that can still be measured is limited. The total number of measurements that can be performed on a single sensor depends on the history of analyte capture, which scales with the analyte concentration and duration of exposure to samples. A shorter exposure time, by using shorter measurements, allows for more samples to be measured, but this comes at the cost of sensitivity. To improve the sensitivity, a BPM sensor can be designed with more particles, so the measurement statistics are higher. In this case the number of particles in the sensor should not only be high, but also stable over time, which may be achieved by control of preparation conditions and flow, by using periodic reversal of flow direction, by re-supply of particles, or by attaching the particles to the surface with a flexible molecular tether (Visser et al., 2018).

We believe that the concepts described in this paper are relevant for BPM as well as for other continuous detection technologies, such as aptamer-based electrochemical sensors (Downs and Plaxco, 2022; Ferguson et al., 2013; Schoukroun-Barnes et al., 2016) and continuous fluorescence-based sensors (Hariri et al., 2023; Thompson et al., 2023). To enable real applications, continuous sensing technologies need to be combined with continuous sampling methods. We have studied integrated sampling-and-sensing using microdialysis and BPM, for the continuous monitoring of cortisol (Smeden et al., 2023). Sampling by microdialysis is advantageous, because commercial catheters can be used, and biomarker molecules are measured in a relatively clean dialysis fluid. We envision a TNF-α monitoring strategy that combines sampling by microdialysis with BPM sensing. The fluidic system will be

fully automated to minimize variabilities and enable robust calibration procedures. Preclinical studies can be performed with complex matrices such as cell culture medium, e.g., for organoid studies. Future clinical implementations may couple to existing blood vessel access points such as intravenous catheters. Finally, it will be interesting to develop strategies for multiplexed sampling-and-sensing, as the ability to measure several biomarkers simultaneously will increase the scope of applications that can be addressed with future sensors for continuous cytokine monitoring, in the fields of fundamental biological research as well as healthcare.

CRediT authorship contribution statement

Alissa D. Buskermolen: Conceptualization, Investigation, Methodology, Validation, Visualization, Writing – original draft, Writing – review & editing. **Claire M.S. Michielsen:** Conceptualization, Methodology, Writing – review & editing. **Arthur M. de Jong:** Conceptualization, Methodology, Supervision, Writing – review & editing. **Menno W.J. Prins:** Conceptualization, Methodology, Supervision, Writing – review & editing.

Declaration of competing interest

The authors declare the following competing financial interest: A.M. d.J. and M.W.J.P. are listed as inventors on patent application WO/2022/039594A1: Biosensor using particle motion. A.D.B. and C.M.S.M. declare no competing interest.

Data availability

Data will be made available on request.

Acknowledgements

We thank Max Bergkamp for the real-time particle tracking algorithms. We thank Stijn Haenen for the custom-built microscopy setups. Part of this work was funded by the Safe-N-Medtech H2020 project under grant agreement number 814607 (A.D.B. and M.W.J.P.). Part of this work was funded by The Netherlands Topsectors Agri&Food, HTSM, and Chemistry under grant project number LWV20.117 (C.M.S.M.).

Appendix A. Supplementary data

Supplementary data to this article can be found online at https://doi.org/10.1016/j.bios.2023.115934.

References

Bergkamp, M.H., Cajigas, S., van Ijzendoorn, L.J., Prins, M.W.J., 2023. High-throughput single-molecule sensors: how can the signals Be analyzed in real time for achieving real-time continuous biosensing? ACS Sens. 8, 2271–2281. https://doi.org/10.1021/acssensors.3c00245.

Buskermolen, A.D., Lin, Y.T., van Smeden, L., van Haaften, R.B., Yan, J., Sergelen, K., de Jong, A.M., Prins, M.W.J., 2022. Continuous biomarker monitoring with single molecule resolution by measuring free particle motion. Nat. Commun. 13, 6052. https://doi.org/10.1038/s41467-022-33487-3.

Cao, C., Zhang, F., Goldys, E.M., Gao, F., Liu, G., 2018. Advances in structure-switching aptasensing towards real time detection of cytokines. Trends Anal. Chem. 102, 379–396. https://doi.org/10.1016/j.trac.2018.03.002.

Chen, P., Huang, N.T., Chung, M.T., Cornell, T.T., Kurabayashi, K., 2015. Label-free cytokine micro- and nano-biosensing towards personalized medicine of systemic inflammatory disorders. Adv. Drug Deliv. Rev. 95, 90–103. https://doi.org/10.1016/j.addr.2015.09.005.

Clifford, A., Das, J., Yousefi, H., Mahmud, A., Chen, J.B., Kelley, S.O., 2021. Strategies for biomolecular analysis and continuous physiological monitoring. J. Am. Chem. Soc. 143, 5281–5294. https://doi.org/10.1021/jacs.0c13138.

Dekkers, J.F., Alieva, M., Cleven, A., Keramati, F., Wezenaar, A.K.L., van Vliet, E.J., Puschhof, J., Brazda, P., Johanna, I., Meringa, A.D., Rebel, H.G., Buchholz, M.B., Barrera Román, M., Zeeman, A.L., de Blank, S., Fasci, D., Geurts, M.H., Cornel, A.M., Driehuis, E., Millen, R., Straetemans, T., Nicolasen, M.J.T., Aarts-Riemens, T., Ariese, H.C.R., Johnson, H.R., van Ineveld, R.L., Karaiskaki, F., Kopper, O., Bar-Ephraim, Y.E., Kretzschmar, K., Eggermont, A.M.M., Nierkens, S., Wehrens, E.J., Stunnenberg, H.G., Clevers, H., Kuball, J., Sebestyen, Z., Rios, A.C., 2023. Uncovering the mode of action of engineered T cells in patient cancer organoids. Nat. Biotechnol. 41, 60–69. https://doi.org/10.1038/s41587-022-01397-w.

Dembic, Z., 2015. The Cytokines of the Immune System. Academic Press. Elsevier. https://doi.org/10.1016/c2013-0-09724-1.

Downs, A.M., Plaxco, K.W., 2022. Real-time, in vivo molecular monitoring using electrochemical aptamer based sensors: opportunities and challenges. ACS Sens. 7, 2823–2832. https://doi.org/10.1021/acssensors.2c01428.

Ferguson, B.S., Hoggarth, D.A., Maliniak, D., Ploense, K., White, R.J., Woodward, N., Hsieh, K., Bonham, A.J., Eisenstein, M., Kippin, T.E., Plaxco, K.W., Soh, H.T., 2013. Real-time, aptamer-based tracking of circulating therapeutic agents in living animals. Sci. Transl. Med. 5, 213ra165. https://doi.org/10.1126/scitranslmed.3007095.

Hariri, A.A., Cartwright, A.P., Dory, C., Gidi, Y., Yee, S., Thompson, I.A.P., Fu, K., Yang, K., Wu, D., Maganzini, N., Feagin, T., Young, B.E., Afshar, B.H., Eisenstein, M., Digonnet, M., Vuckovic, J., Soh, H.T., 2023. Modular aptamer switches for the continuous optical detection of small-molecule analytes in complex media. Adv. Mater. 2304410 https://doi.org/10.1002/adma.202304410.

Kany, S., Vollrath, J.T., Relja, B., 2019. Cytokines in inflammatory disease. Int. J. Mol. Sci. 20 https://doi.org/10.3390/ijms20236008.

Kiers, D., Leijte, G.P., Gerretsen, J., Zwaag, J., Kox, M., Pickkers, P., 2019. Comparison of different lots of endotoxin and evaluation of in vivo potency over time in the experimental human endotoxemia model. Innate Immun. 25, 34–45. https://doi.org/10.1177/1753425918819754.

Kox, M., Van Eijk, L.T., Zwaag, J., Van Den Wildenberg, J., Sweep, F.C.G.J., Van Der Hoeven, J.G., Pickkers, P., 2014. Voluntary activation of the sympathetic nervous system and attenuation of the innate immune response in humans. Proc. Natl. Acad. Sci. U.S.A. 111, 7379–7384. https://doi.org/10.1073/pnas.1322174111.

Landry, J.P., Ke, Y., Yu, G.L., Zhu, X.D., 2015. Measuring affinity constants of 1450 monoclonal antibodies to peptide targets with a microarray-based label-free assay platform. J. Immunol. Methods 417, 86–96. https://doi.org/10.1016/j.jim.2014.12.011.

Liu, B.M., Martins, T.B., Peterson, L.K., Hill, H.R., 2021. Clinical significance of measuring serum cytokine levels as inflammatory biomarkers in adult and pediatric COVID-19 cases: a review. Cytokine. https://doi.org/10.1016/j.cyto.2021.155478.

Liu, C., Chu, D., Kalantar-Zadeh, K., George, J., Young, H.A., Liu, G., 2021. Cytokines: from clinical significance to quantification. Adv. Sci. 8, 2004433 https://doi.org/10.1002/advs.202004433.

Lubken, R.M., Bergkamp, M.H., de Jong, A.M., Prins, M.W.J., 2021. Sensing methodology for the rapid monitoring of biomolecules at low concentrations over long time spans. ACS Sens. 6, 4471–4481. https://doi.org/10.1021/acssensors.1c01991.

Marshall, J.S., Warrington, R., Watson, W., Kim, H.L., 2018. An introduction to immunology and epigenetics. Allergy Asthma Clin. Immunol. 14, 1–23. https://doi.org/10.1016/B978-0-12-817964-2.09991-3.

Martens, K.J.A., Bader, A.N., Baas, S., Rieger, B., Hohlbein, J., 2018. Phasor based single-molecule localization microscopy in 3D (pSMLM-3D): an algorithm for MHz localization rates using standard CPUs. J. Chem. Phys. 148, 123311 https://doi.org/10.1063/1.5005899.

Netea, M.G., Schlitzer, A., Placek, K., Joosten, L.A.B., Schultze, J.L., 2019. Innate and adaptive immune memory: an evolutionary continuum in the host's response to pathogens. Cell Host Microbe 25, 13–26. https://doi.org/10.1016/J.CHOM.2018.12.006.

Roberts, G.C.K. (Ed.), 2013. Encyclopedia of Biophysics, first ed. Springer Berlin, Heidelberg. https://doi.org/10.1007/978-3-642-16712-6.

Schoukroun-Barnes, L.R., Macazo, F.C., Gutierrez, B., Lottermoser, J., Liu, J., White, R.J., 2016. Reagentless, structure-switching, electrochemical aptamer-based sensors. Annu. Rev. Anal. Chem. 9, 163–181. https://doi.org/10.1146/annurev-anchem-071015-041446.

Smeden, L. van, de Jong, A.M., Prins, M.W.J., 2023. Integrated sampling-and-sensing using microdialysis and Biosensing by Particle Motion for continuous cortisol monitoring. Sens. Diagnost. 2, 1638–1648. https://doi.org/10.1039/D3SD00185G.

Thompson, I.A.P., Saunders, J., Zheng, L., Hariri, A.A., Maganzini, N., Cartwright, A.P., Pan, J., Yee, S., Dory, C., Eisenstein, M., Vuckovic, J., Soh, H.T., 2023. An antibody-based molecular switch for continuous small-molecule biosensing. Sci. Adv. 9, eadh4978 https://doi.org/10.1126/sciadv.adh4978.

Visser, E.W.A., Yan, J., Van Ijzendoorn, L.J., Prins, M.W.J., 2018. Continuous biomarker monitoring by particle mobility sensing with single molecule resolution. Nat. Commun. 9, 2541. https://doi.org/10.1038/s41467-018-04802-8.

Yang, D., Singh, A., Wu, H., Kroe-Barrett, R., 2016. Comparison of biosensor platforms in the evaluation of high affinity antibody-antigen binding kinetics. Anal. Biochem. 508, 78–96. https://doi.org/10.1016/j.ab.2016.06.024.

Yiu, H.H., Graham, A.L., Stengel, R.F., 2012. Dynamics of a cytokine storm. PLoS One 7, e45027. https://doi.org/10.1371/journal.pone.0045027.